°C (δ 67.6 ppm) as secondary standards. ^{31}P NMR spectra were recorded on a Varian XL-400 spectrometer at 161.82 MHz and referenced to free HMPA set at δ 26.4 ppm according to Reich. NMR probe temperatures are accurate to ±2 °C. The shims were adjusted using ^1H line shape and free-induction decays rather than using the deuterium lock solvent to maximize field homogeneity. Resolution enhancements were performed by Lorentz–Gaussian multiplication of the FID prior to Fourier transformation. The hardware modifications necessary for single frequency irradiations are described elsewhere.[17]

The following is a representative procedure for preparing samples for NMR spectroscopic analysis. Working in an inert atmosphere glovebox [^6Li,^{15}N]LiTMP (0.103 g, 0.70 mmol) and diphenylacetic acid (200 mg, 0.942 mmol) were added to separate serum vials containing stir fleas and capped with serum stoppers. An additional serum vial fitted with a stir flea and serum cap, the three samples prepared previously, and four NMR tubes fitted with serum stoppers were removed from the glovebox and placed under positive helium pressure with needle inlets connected to a He/vacuum double manifold. (Helium is used to prevent explosions due to gas condensation). To the vial containing the [^6Li,^{15}N]LiTMP cooled to −78 °C was added THF (1.40 mL) down the walls with constant agitation to minimize local heating. Solutions of HMPA (1.30 M) and diphenylacetic acid (0.0942 M) were prepared by bringing the volumes to 10.0 mL with dry THF (accounting for the volume of the stir flea). The LiTMP titer was determined by adding 0.50 mL of the LiTMP stock solution to 0.5 mL of THF in the last serum vial and titrated to a yellow-to-colorless endpoint with diphenylacetic acid in THF. The NMR tubes at 77 K were each charged with 250 μL of dry pentane, 0.098 mmol of the [^6Li,^{15}N]LiTMP stock solution, variable quantities of the HMPA stock solution, and enough THF to result in a final volume of 750 μL. Samples were flame sealed at 77 K under reduced pressure and stored at 77 K until the spectroscopic analyses were initiated.

Acknowledgment. We are indebted to H. J. Reich and L. M. Jackman for many enlightening discussions and W. H. Saunders, P. v. R. Schleyer, S. E. Denmark, and R. Snaith for copies of manuscripts prior to publication. We acknowledge the National Science Foundation Instrumentation Program (CHE 7904825 and PCM 8018643), the National Institutes of Health (RR02002), and IBM for support of the Cornell Nuclear Magnetic Resonance Facility. We also thank the National Institutes of Health for direct support of this work.

Supplementary Material Available: ^{15}N NMR spectra of [^6Li,^{15}N]LDA/HMPA, ^{31}P NMR spectra of [^6Li]LDA/HMPA and [^6Li]LiTMP/HMPA, and single frequency decouplings of [^6Li,^{15}N]LiTMP/HMPA (5 pages). Ordering information is given on any current masthead page.

Distorted Amides as Models for Activated Peptide N–C(O) Units. 3. Synthesis, Hydrolytic Profile, and Molecular Structure of 2,3,4,5-Tetrahydro-2-oxo-1,5-propanobenzazepine

Q.-P. Wang,[†] A. J. Bennet,[†] R. S. Brown,*[,†] and B. D. Santarsiero[‡]

Contribution from the Department of Chemistry and Structure Determination Laboratory, Department of Chemistry, University of Alberta, Edmonton, Alberta, Canada.
Received December 18, 1990

Abstract: A distorted amide (2,3,4,5-tetrahydro-2-oxo-1,5-propanobenzazepine (**1d**)) was synthesized and its structure determined by X-ray diffraction. The amidic unit of **1d** is compared with that found in undistorted *p*-bromo-*N*,2-dimethylacetanilide (**3b**) and more distorted 2,3,4,5-tetrahydro-2-oxo-1,5-ethanobenzazepine (**1b**) and 3,4-dihydro-2-oxo-1,4-propanoquinoline (**1c**). The progressive distortion manifests itself in a lengthening of the N—C(O) bond, a slight shortening of the C=O bond, and a twisting about the N—C(O) unit with attendent rehybridization of the N from sp^2 to sp^3 and a slight pyramidalization of the (N)(C)C=O unit. The hydrolysis of **1d** in D_2O and H_2O is compared with those of *N*-methylacetanilide (**3a**), **1b**, **1c**, and **1a** (3,4-dihydro-2-oxo-1,4-ethanoquinoline), the most distorted anilide in the series. In passing from **3a** to **1a**, the attack of OH^- is accelerated by roughly 7 orders of magnitude, while the acid-catalyzed hydrolysis is accelerated by 11 orders of magnitude. Based on the solvent kinetic isotope effects, pH/rate profiles, and activation parameters, a unified mechanism for H_3O^+- and OH^--promoted hydrolysis of these anilides is proposed. The effect of varying [acetate] in catalyzing the hydrolysis of **1b** and **1c** in H_2O and D_2O as a function of pL was studied and analyzed in terms of a specific-acid/general-base process involving acetate-promoted delivery of L_2O on protonated amide.

Introduction

Structural distortion of an amide unit away from planarity has been shown to markedly alter its spectroscopic properties and kinetic reactivity toward nucleophilic attack/hydrolysis.[1-3] Recent work from these laboratories[3] has concentrated on the relationship between hydrolytic reactivity and amidic distortions that involve (1) rotation about and lengthening of the N—C(O) bond and (2) N-pyramidalization. In these studies it was shown that both factors accelerate the attack of nucleophiles on the C=O unit of molecules such as **1a–c** and **2**. Moreover, it was demonstrated that the amidic distortion inherent in **1b** predisposes it toward attack by bifunctional nucleophiles such as β-amino alcohols[3b-d] and diacids capable of forming cyclic anhydrides[3e] in a way that is reminiscent of the serine proteases and aspartate proteinases, respectively.

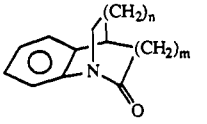

1a n=m=1
b n=1, m=2
c n=2, m=1
d n=m=2

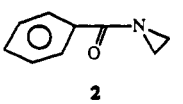

2

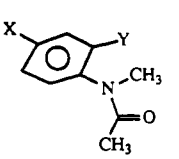

3a X=Y=H
b X=Br, Y=CH_3

[†] Department of Chemistry.
[‡] Structure Determination Laboratory, Department of Chemistry.

(1) (a) Pracejus, H. von; Kehlen, M.; Kehlen, H.; Matschiner, H. *Tetrahedron* **1965**, *21*, 2257. (b) Pracejus, H. von *Chem. Ber.* **1959**, *92*, 988. (c) Kostyanovskii, R. G.; Mikhlina, E. E.; Levkoeva, E. I.; Yakhontov, L. N. *Org. Mass. Spectrom.* **1970**, *3*, 1023.

0002-7863/91/1513-5757$02.50/0

The above studies have possible implications for a variety of biological and enzyme-mediated acyl-transfer processes. It is appropriate to establish a more quantitative relationship between the degree of amide distortion and susceptibility toward hydrolysis as demonstrated by structural and kinetic studies. The bicyclic anilides (**1**) provide one such homologous series in which elongation of the benzylic C,N bridges allows the N to relax from a nearly orthogonal sp^3 configuration (**1a**) toward a nearly sp^2-conjugated one as in **1d**. Herein we provide structural details of **1d** and **3b** that can be compared with those of distorted **1b**[3b] or **1c**,[3g] as well as the thermodynamic parameters and kinetics for hydrolysis of **1a–d**[4] and **3a** in aqueous media. In addition, we report a detailed study of the effect of acetate ion in catalyzing the hydrolysis of **1b,c** in H_2O and D_2O under acidic conditions.

Experimental Section

(a) Materials. Amides **1a–c** were synthesized as previously described.[3a,f] *N*-Methylacetanilide was commercial.

***p*-Bromo-*N*,2-dimethylacetanilide (3b)** was prepared by a standard methodology described in the supplementary material: mp 93.5–94.5 °C; ^{1}H NMR (300 MHz, $CDCl_3$) δ 7.46 (1 H, d, J = 2 Hz), 7.39 (1 H, dd, J = 2, 8 Hz), 7.01 (1 H, d, J = 8 Hz) and two sets of three singlets each (100:3.5 = *E*:*Z*), major isomer δ 3.14 (NMe), 2.20 (ArMe), 1.75 (C(O)Me), minor isomer δ 3.26 (NMe), 2.26 (ArMe), 2.16 (C(O)Me); ^{13}C NMR (75 MHz, $CDCl_3$) δ 170.39 (C(O)), 142.20, 137.74, 133.34, 130.67, 129.53, 121.95, 35.80, 21.91, 17.18; mass spectrum, m/z 243, 241 (M^+), 228, 226, 201, 200, 199, 198, 186, 184, 56 (base peak); FTIR ($CHCl_3$ cast) 1647.7 cm^{-1}. Anal. C, H, N.

The preparation of **1d** was accomplished according to the route outlined in Scheme I starting with the known *N*-tosyl acid **4**.[3f]

5-(2-Carboxyethyl)-*N*-tosyl-2,3,4,5-tetrahydrobenzazepine (5). To a 200-mL round-bottomed flask were added 8.6 g (24 mmol) of **4**,[3e] 17.5 mL (240 mmol) of thionyl chloride, and 50 mL of dry benzene. The mixture was heated at reflux overnight, after which an additional 5 mL of $SOCl_2$ was added followed by heating at reflux for 1 h. The volatiles were removed by rotary evaporation, and then 50 mL of benzene was added and evaporated. The latter process was repeated to remove traces of $SOCl_2$. The resulting acid chloride exhibited an IR absorbance at 1802 cm^{-1} (film).

The acid chloride was immediately placed in a 250-mL dropping funnel along with 200 mL of dry ether. It was then added dropwise to a solution of ~3 g of diazomethane in 130 mL of ether (prepared from Diazald as reported[5]) that had been cooled to 0 °C in an ice bath. After complete addition, the mixture was allowed to stand for 2 h. The excess CH_2N_2 was removed by distilling (bath temperature 50–60 °C) an amount of ether sufficient to afford a colorless distillate after which the remaining volatiles were removed by rotary evaporation to yield an oil: IR (film) 2120 cm^{-1}.

The diazomethane addition product from above was immediately placed into a dropping funnel containing 40 mL of 1,4-dioxane. The contents were then added over a 20-min period to a 500-mL flask containing a stirred mixture of 0.28 g of silver oxide, 0.70 g of anhydrous sodium carbonate, 0.42 g of sodium thiosulfate, and 30 mL of water at 60–65 °C. Following the addition, the contents of the flask were heated at 90 °C for 5 h during which time a mixture of silver oxide (0.28 g), sodium carbonate (0.7 g), sodium thiosulfate (0.42 g), 30 mL of water, and 15 mL of dioxane was added after each hour.

The pH of the reaction mixture was then adjusted to 1.0 with 1.0 N HNO_3, and the resultant was then extracted with 3 × 100 mL of $CHCl_3$. The combined organics were dried ($MgSO_4$) and filtered and the volatiles removed by rotary evaporation to yield 8.0 g of crude **5**. It was purified by dissolution in 200 mL of 1 N NaOH. The basic solution was extracted with 3 × 100 mL of CH_2Cl_2 and the water layer decolorized with charcoal. The solution was made acidic by addition of concentrated HCl which induced precipitation. The solid was collected and dissolved in a minimum amount of 95% EtOH, and then water was added to turbidity. After refrigeration, a white solid was collected and dried to yield 4.36 g of pure **5** (49% based on **4**): mp 152.2–153.3 °C; ^{1}H NMR (200 MHz, $CDCl_3$) δ 7.1–7.8 (8 H, br), 3.3–4.1 (2 H, br), 2.5 (5 H, br), 2.2 (3 H, s), 2.0–1.2 (4 H, br); NH_4^+ chemical ionization mass spectrum, m/z 391 (100%, M^+ + 18). Anal. C, H, N.

5-(2-Carboxyethyl)-2,3,4,5-tetrahydrobenzazepine (6). To a 500-mL round-bottomed flask fitted with a dry ice condenser and gas inlet tube were added 2.0 g (5.36 mmol) of **5** and 50 mL of dry THF, and the solution was then cooled to −50 °C. Into this was condensed ~200 mL of NH_3. Sodium metal was added portionwise until a persistent blue color was obtained. The mixture was stirred for an additional 10 min after which solid NH_4Cl was added in small portions until the mixture was colorless. After evaporation of the NH_3 (ambient conditions), the solution was acidified with 1 N HCl and then extracted with 3 × 50 mL of benzene. The latter benzene extracts were combined, dried ($MgSO_4$), and filtered and the volatiles removed to yield 1.1 g of crude **6**. It was purified by recrystallization from 95% EtOH/H_2O to yield 0.61 g (52%) of pure **6**: mp 129–130 °C; ^{1}H NMR (200 MHz, $CDCl_3$) δ 7.32 (2 H, br), 7.03 (2 H, dd, J_1 = 5 Hz, J_2 = 7 Hz), 6.84 (1 H, dd, J_1 = 7 Hz, J_2 = 2 Hz), 6.70 (1 H, d, J = 7 Hz), 3.26 (1 H, m), 2.83 (2 H, m), 2.10–2.40 (3 H, m), 1.60–2.00 (5 H, m); mass spectrum, m/z 219.1258 (calcd for $C_{13}H_{17}NO_2$, 219.1259). Anal. C, H, N.

2,3,4,5-Tetrahydro-2-oxo-1,5-propanobenzazepine (1d). To a 500-mL three-necked round-bottomed flask were added 200 mL of dry CH_3CN (distilled from P_2O_5) and 0.50 g (2.28 mmol) of amino acid **6**. The mixture was stirred until all solids dissolved after which 0.50 g (2.42 mmol) of dicyclohexylcarbodiimide in 2.5 mL of dry CH_3CN was added by syringe. The solution was allowed to stand overnight and periodically monitored by IR spectroscopy to observe the appearance of a C=O band at ~1680 cm^{-1}. After complete reaction, the mixture was filtered (to remove dicyclohexylurea) and the volatiles were removed by rotary evaporation. The solid residue was redissolved in a small amount of dry benzene, filtered to remove the last traces of dicyclohexylurea, and then stripped of benzene. The so-obtained solid was recrystallized from octane to yield 0.41 g (89%) of pure amide **1d**: mp 82.3–83.3 °C; ^{1}H NMR (200 MHz, $CDCl_3$) δ 7.35 (2 H, m), 7.15 (2 H, m), 4.52 (1 H, ddd, J_1 = 2 Hz, J_2 = 13 Hz, J_3 = 6 Hz), 3.10–3.24 (1 H, m), 2.90 (1 H, dd, J_1 = 6 Hz, J_2 = 13 Hz), 2.10–2.32 (5 H, m), 1.50–1.70 (2 H, m), 1.24–1.36 (1 H, m); ^{13}C NMR (85 MHz, $CDCl_3$) δ 180.39, 141.24, 139.37, 128.38, 127.97, 127.72, 126.29, 47.67, 38.44, 38.26, 32.23, 28.96, 25.44; IR (FTIR, $CHCl_3$ cast) 1676.6 cm^{-1}; mass spectrum, m/z 201.1146 (calcd for $C_{13}H_{15}NO$, 201.1154). Anal. C, H, N.

(b) Kinetics. Triply distilled H_2O was used throughout. Kinetic data for the hydrolysis of **1d** were obtained at 25.0 °C by measuring the rate of change of absorbance of 2.67 × 10^{-4} M aqueous solutions of **1d** at the wavelength of maximum change (230 nm for pH <3.0, 240 nm for pH >12) with a Hewlett-Packard 8451A diode array UV–vis spectrophotometer. Buffers employed were HCl (pH ≤3) and NaOH (pH ≥12.0). The reactions were initiated by injecting 10 μL of an 80 mM stock solution of **1d** in CH_3CN into 3.0 mL of the buffer (μ = 1.0 KCl) in a 1.0-cm path length quartz cuvette that had been thermally equilibrated in the spectrophotometer cell holder for 30 min. All reactions were followed in triplicate and monitored for at least 3 half-lives except for those at pH 2.7 and 3.0 which were followed to 2 half-lives. The end points for the latter two slow reactions were determined by measuring the absorbance at 230 or 240 nm of a 2.67 × 10^{-4} M aqueous solution of authentic amino acid **6** in the same medium. Pseudo-first-order rate constants (k_{obsd}) were evaluated by a nonlinear least-squares fitting of the absorbance vs time data to a standard exponential model. pH measurements were made with a Radiometer TTT2 titration unit in conjunction with a Radiometer GK-2321C combination electrode standardized prior to use with certified pH 4.00, 7.00, and 10.00 buffers. [H_3O^+] at pH values less than 2 or greater than 12 were determined by titration with standardized NaOH or HCl, respectively, with use of bromothymol blue as an indicator.

(c) Product Analysis. Into 3.0 mL of pH 0.0 HCl buffer was injected 10 μL of 80 mM **1d** in CH_3CN. The UV spectrum was monitored from 220 and 300 nm continuously for the time course of the reaction by a Cary 210 UV–vis spectrophotometer. An isosbestic point at λ = 250 nm was observed. At the completion of the run, the λ_{max} at 230 nm had an ϵ = 2820 M^{-1} cm^{-1} and the overall spectrum was superimposable upon that of an authentic 2.67 × 10^{-4} M solution of authentic **6** in 1.0 M HCl.

(d) D_2O Studies. Solvent kinetic isotope studies for **1a–c** were conducted at 25.0 °C and 290 nm on a Durrum-Gibson stopped-flow spectrophotometer under acidic and basic conditions. Into one drive syringe was placed an 0.2 M NaOD solution (μ = 1.0 KCl) or 2 × 10^{-2} M DCl (μ = 1.0 KCl) solution. The second syringe contained D_2O (μ = 1.0 KCl)

(2) (a) Blackburn, G. M.; Plackett, J. D. *J. Chem. Soc., Perkin Trans. 2* **1973**, 981; **1972**, 1366. (b) Blackburn, G. M.; Skaife, C. J.; Kay, I. T. *J. Chem. Res., Miniprint* **1980**, 3650.

(3) (a) Somayaji, V.; Brown, R. S. *J. Org. Chem.* **1986**, *51*, 2676. (b) Somayaji, V.; Skorey, K. I.; Brown, R. S.; Ball, R. G. *J. Org. Chem.* **1986**, *51*, 4866. (c) Somayaji, V.; Skorey, K. I.; Brown, R. S. *J. Am. Chem. Soc.* **1988**, *110*, 5205. (d) Skorey, K. I.; Somayaji, V.; Brown, R. S. *Ibid.* **1989**, *111*, 1445. (e) Somayaji, V.; Keillor, J.; Brown, R. S. *Ibid.* **1988**, *110*, 2625. (f) Wang, Q.-P.; Bennet, A. J.; Brown, R. S. *Can. J. Chem.* **1990**, *68*, 1732. (g) Bennet, A. J.; Wang, Q.-P.; Slebocka-Tilk, H.; Somayaji, V.; Brown, R. S.; Santarsiero, B. D. *J. Am. Chem. Soc.* **1990**, *112*, 6383. (h) Slebocka-Tilk, H.; Brown, R. S. *J. Org. Chem.* **1987**, *52*, 805.

(4) The pH/rate constant profiles for **1a**,[2c,3a] **1b**,[3a] and **1c**[3f] at 25 °C have been reported.

(5) Fieser, L. F.; Fieser, M. *Reagents for Organic Synthesis*; Wiley: New York, 1967; Vol. 1, pp 191–192.

Table I. Experimental Details of Intensity Data Collection and Refinement of **1d** and **3b**

	Crystal Data	
formula	$C_{13}H_{15}NO$	$C_{10}H_{12}BrNO$
formula weight	201.27	242.12
crystal dimens, mm	0.3, 0.3, 0.3	0.23, 0.26, 0.46
space group	$P2_1/n$	$Pna2_1$
a, Å	9.020 (3)	11.305 (7)
b, Å	10.177 (4)	10.217 (5)
c, Å	22.663 (10)	9.144 (3)
β, deg	93.72 (3)	
V, Å^3	2075	1056
Z	8	4
D_c, g cm^{-3}	1.285	1.523
μ, cm^{-1}	0.76	38.15
	Data Collection	
radiation	Mo Kα	Mo Kα
wavelength, Å	0.7107	0.7107
monochromator	graphite	graphite
scan type	θ–2θ	θ–2θ
scan rate, deg min^{-1}	1.0–2.0	2.0
scan width, deg	0.40–0.60 + tanθ	1.00 + tanθ
2θ(max), deg	40	56
index range	$h,\pm k,\pm l$	$\pm h,\pm k,\pm l$
reflections, averaged	3877	2805
	Refinement	
observations/variables	1434/271	1455/117
discrimination criteria	$I > 2\sigma(I)$	$I > 3\sigma(I)$
absorption	empirical	empirical
R_1	0.055	0.031
R_2	0.055	0.033
goodness-of-fit	1.29	1.04

along with ~3 × 10^{-4} M **1a–c**. Reactions were monitored to completion in triplicate. The final [OD$^-$] or [D_3O^+] was determined by titration of the effluent from the spectrophotometer cell by standardized HCl or NaOH titrants and bromothymol blue indicator. For **1d**, which reacts more slowly than any of **1a–c**, the solvent isotope effects were determined on a Cary 210 UV–vis spectrophotometer at 25 °C and λ = 240 nm (1.06 M NaOD) or λ = 230 nm (pD = 2.18).

(e) Acetate Buffer Effects on the Hydrolysis of 1b,c in H_2O and D_2O at 25.0 °C. Anhydrous NaOAc (GIC), MES (2-*N*-morpholinoethanesulfonic acid), and D_2O (Merck) were used without further purification. Throughout its useful buffering range (pL values between pK_a + 1 and pK_a − 1; L = H, D) acetate was used as the buffer. Above pL readings of pK_a + 1, the pL was controlled by 0.05 M MES to which was added acetate. pL readings of the solutions before and after the kinetic determinations indicated no changes in excess of 0.02 unit. pD values were determined by adding 0.4 unit[6,7] to the pH meter reading. Pseudo-first-order rate constants (k_{obsd}) for the disappearance of **1b** (291 nm) and **1c** (260 nm) were determined in triplicate at each pL as a function of total acetate concentrations varying between 50 and 200 mM (μ = 1.0 KCl). Second-order rate constants were evaluated from the slopes of the k_{obsd} values vs [acetate]$_{total}$. The pK_a^D for DOAc was taken from a literature value (5.25, μ = 0, 25 °C)[7] and corrected[8] to a value of 5.05 (25 °C) at μ = 1.0.

(f) Crystal and Molecular Structure of 1d and 3b. A crystal of **3b** suitable for X-ray diffraction studies was grown by allowing a saturated (30 °C) solution of the amide in 2-methylbutane to stand at room temperature for several days. Suitable crystals of **1d** were grown from a saturated 50:50 ethanol/H_2O solution that was allowed to stand overnight at room temperature. Given in Table I are the experimental details for amides **1d** and **3b**. Full X-ray crystallographic details for **1d** and **3b** are available as Tables 1S and 2S (supplementary material).

Results

Structure. Amide **1d** was prepared in 22.6% overall yield from **4**[3g] by the route shown in Scheme I. Amide **3b** was chosen for comparison with the bicyclic amides because it was anticipated to have a planar amidic unit, but the plane of the amide should be rotated ~90° relative to the aromatic ring by virtue of buttressing with the ortho CH_3 group. The unit cell of **1d** was found to contain two crystallographically independent molecules as does

Scheme I. Synthetic Route for Preparation of **1d**

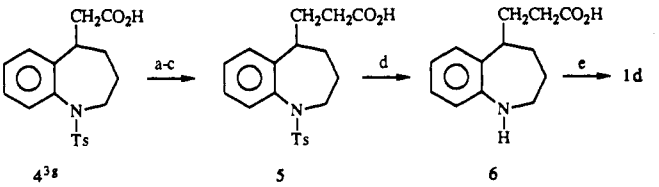

4[3g] **5** **6**

[a] (a) Key: $SOCl_2$/benzene/12 h; (b) CH_2N_2/ether–benzene; (c) $Ag_2O/Na_2CO_3/Na_2S_2O_3/H_2O$; (d) Na/NH_3/−33 °C; (e) DCC/CH_3CN.

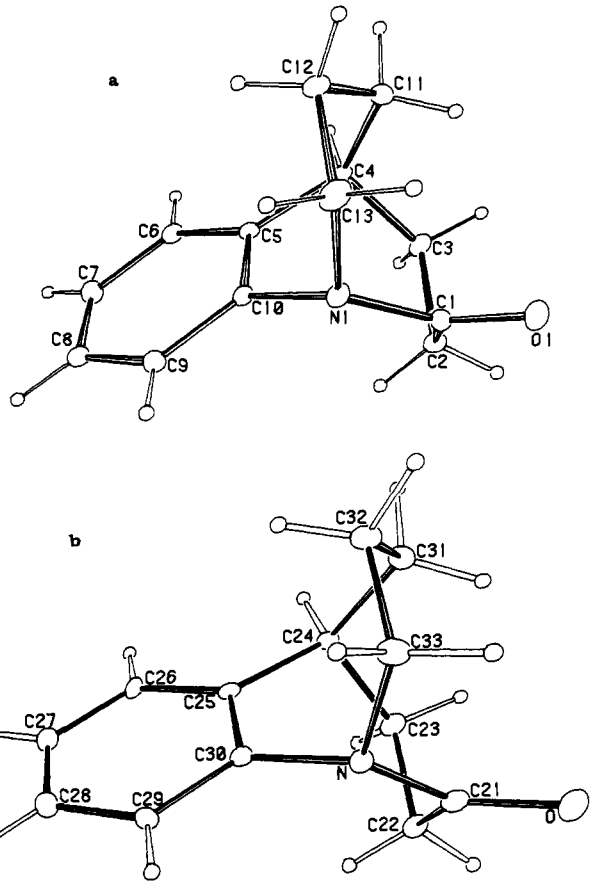

Figure 1. Perspective views of the two crystallographically independent molecules of **1d** in the unit cell. Atoms are represented by Gaussian ellipsoids at the 20% probability level. (Atom numbering is for crystallographic purposes only and does not correspond to naming of the compound.)

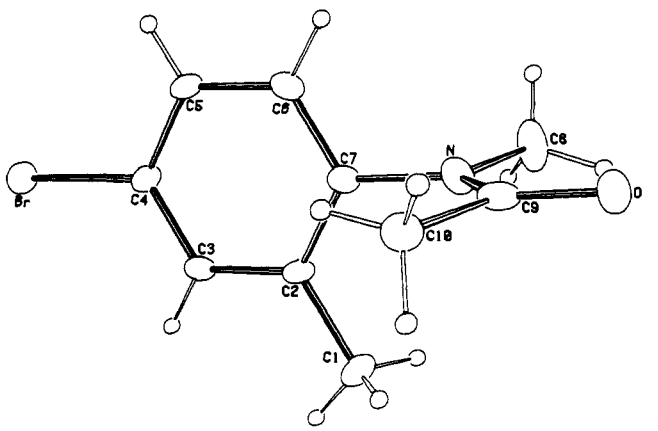

Figure 2. Perspective view of **3b**. Atoms are represented by Gaussian ellipsoids at the 20% probability level.

the unit cell of **1c**.[3f] Given in Figures 1a,b and 2 are the perspective views and atom numberings of the two forms of **1d** and that of

(6) Fife, T. H.; Bruice, T. C. *J. Phys. Chem.* **1961**, *65*, 1079.
(7) Glasoe, P. K.; Long, F. A. *J. Phys. Chem.* **1960**, *64*, 188.
(8) Alberts, A.; Seargent, E. P. *The Determination of Ionization Constants*, 3rd ed.; Chapman and Hall: London, 1984; p 50.

Table II. Selected Structural Parameters for Anilides **1b–d** and **3b**

amide	r(N—C(O)), Å	r(C=O), Å	N—C(O)—C, deg	Dunitz parameters[a] χ_C	χ_N	τ'	twist[b] angle, deg	tilt[b] angle, deg
1b[c]	1.401 (2)	1.216 (2)	116.5 (1)	9.0	57.2	71.2	30.7	15.2
1c[d,e]	1.413 (10)	1.225 (7)	116.9 (5)	11.0	52.8	75.6	33.2	16.0
	1.419 (11)	1.233 (10)	117.0 (7)	6.7	55.1	82.4	38.9	16.8
1d[e]	1.370 (6)	1.233 (6)	116.3 (4)	4.3	38.6	34.4	15.3	10.5
	1.374 (6)	1.241 (6)	116.9 (5)	3.8	38.3	37.8	17.1	10.6
3b	1.338 (7)	1.235 (6)	118.1 (5)	−1.5	3.7	1.3	1.5	1.0

[a] Reference 9. [b] Defined as in ref 11. [c] Reference 3b. [d] Reference 3f. [e] Two crystallographically independent molecules in unit cell.

Table III. Rate and Dissociation Constants for the Hydrolysis of Amides **1a–d** and **3a** in H_2O (T = 25 °C, μ = 1.0 (KCl)

compd	k_1, s^{-1}	pK_a'	k_2, s^{-1}	k_3, $M^{-1}\ s^{-1}$	k_1/K_a', $M^{-1}\ s^{-1}$
1a[a]	4.45 ± 0.22	3.71 ± 0.05	(2.02 ± 0.11) × 10^{-3}	(2.62 ± 0.20) × 10^2 (2.39 ± 0.05) × 10^{2}[b]	(2.28 ± 0.16) × 10^4
1b[c]	101 ± 7	−0.28 ± 0.03		60 ± 1 62 ± 2[b]	56 ± 3[d]
1c	8.3 ± 1.7	0.56 ± 0.05		17.2 ± 1.7 13.1 ± 0.2[b]	29.5 ± 1.5[d]
1d				(5.12 ± 0.02) × 10^{-4} (5.26 ± 0.04) × 10^{-4}[b]	(1.21 ± 0.02) × 10^{-4}
3a				(2.2 ± 0.1) × 10^{-5}	(2.2 ± 0.2) × 10^{-7}

[a] Reference 3a. [b] In D_2O/OD^-. [c] Reference 3f. [d] Errors on k_1 and pK_a' are obtained from the fits of the k_{obsd} vs $[H^+_3O]$ data to eq 3. Errors on k_1/K_a' obtained from linear least-squares analysis of first-order section of the k_{obsd} vs $[H_3O^+]$ plot. [e] Extrapolated to 25 °C from activation parameters in Table IV.

3b. Full crystallographic details are given as supplementary material. At present, we have been unable to obtain crystals of **1a** satisfactory for X-ray crystallographic analysis.[9]

In general, **1b**,[3b] **c**,[3f,g] **d**, and **3b** display bond distances and angles within normal limits. The fragments of interest in each are those containing the heavy atoms of the amide linkage. Selected bond distances and angles, Dunitz parameters (χ_C, χ_N, τ'),[10] and twist and tilt angles[11] for these amides are given in Table II.

The data indicate that in passing from essentially undistorted **3b** to progressively more distorted **1d** → **1b,c**, there is a lengthening of the N—C(O) bond by some 0.06–0.08 Å, while the C=O bond length is scarcely affected, the overall decrease being ~0.02 Å. As well, in passing from **3b** through the series, there is an increase in the molecular distortion of the amidic unit characterized by N-pyramidalization (χ_N,[10] tilt angle[11]) and rotation about the N—C(O) bond (τ',[10] twist angle[11]). Accompanying the molecular deformation is a very slight pyramidalization of the carbonyl carbon. This is quantitatively assessed relative to the N, O, C_2 plane (N, O, C_{10} in the case of **3b**) as the vertical displacement: **3b**, 0.011 Å; **1d**, 0.030 Å; **1c**, 0.079 Å; **1b**, 0.064 Å. In the bicyclic amides, each C(O) carbon is displaced in the direction away from the opposite ethano or propano bridge and toward the underside of the molecule closest to the aromatic ring.

Hydrolysis of 1a–d and 3a. The pH/log k_{hyd} profiles for **1a–d** at 25 °C (μ = 1.0, KCl) are shown in Figure 3. Each amide shows domains that are first order in $[OH^-]$ and first order in $[H_3O^+]$. Additionally, **1a** shows a domain between pH 7 and 9 that is pH independent and attributable to H_2O attack on neutral **1a**, or its kinetic equivalent, OH^- attack on **1a**-H^+. The plateau for **1a** below pH 3.5 is attributable to H_2O attack on an N-protonated form.[3a] Two of the less distorted amides (**1b,c**) also show evidence of

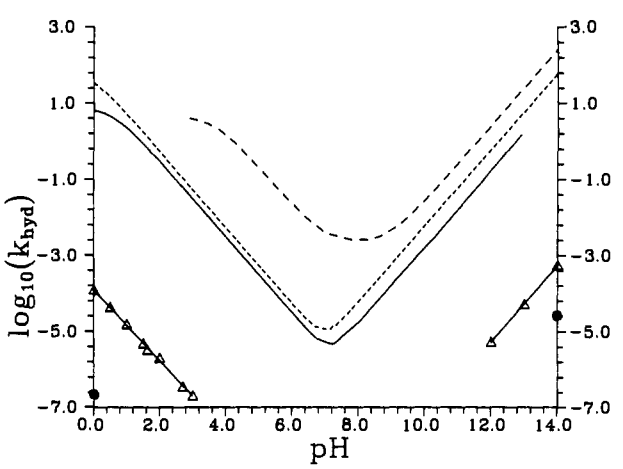

Figure 3. pH/log k_{hyd} profiles for the hydrolysis of **1a–d** in aqueous media (μ = 1.0 (KCl), T = 25.0 ± 0.2 °C): **1a**, ––; **1b**, - - -; **1c**, —; **1d**, △; **3a**, ●.

plateaus, but these appear only at high $[H_3O^+]$,[3f] attesting to the lower pK_a for their protonated forms: no evidence for any water reaction is seen at neutral pH. Of the bicyclic anilides, **1d** is the least distorted and kinetically the least reactive. Due to the slowness of its hydrolysis at 25 °C, the kinetics could only be monitored between pH 0–3 and 12–14. Finally, shown by the closed circles on Figure 3 at pH 0 and 14 are hydrolytic rate constants for **3a** extrapolated from higher temperature data to 25 °C.

The appearance of the profiles given in Figure 3 suggests a generalized hydrolytic mechanism for these amides, formulated as in eq 1 where P represents the product amino acid or amine + acid and A-H^+ represents the protonated amide without des-

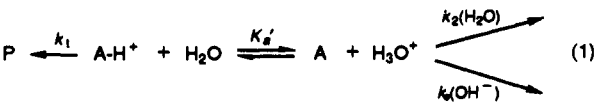

(1)

ignation of the site. In eq 2 is given the generalized rate constant

$$k_{hyd} = \frac{k_1[H^+]^2 + k_2K_a'[H^+] + k_3K_aK_w}{[H^+]^2 + K_a'[H^+]} \quad (2)$$

expression that obtains for **1a** where $K_w = 10^{-14}$. For **1b,c**, which show no evidence for a water reaction, the expression simplifies

(9) We have managed to obtain crystals of the *p*-chloro derivative of **1a** that are of sufficient quality for X-ray analysis. Preliminary investigations indicate that this derivative has $\chi_C = 2 \pm 2°$, $\chi_N = -64 \pm 2°$, $\tau' = -173 \pm 10°$, twist angle 5 ± 5°, and tilt angle 21 ± 5°. Further refinement of the structure is necessary before conclusions regarding bond lengths can be made. Santarsiero, B. D.; Huang, X.; Brown, R. S. Unpublished results.

(10) Dunitz, J. D.; Winkler, F. K. *Acta Crystallogr.* **1975**, *B31*, 251.

(11) While the most precise description of molecular distortion obtains from the analysis of the atomic positions proposed by Dunitz and Winkler,[10] a qualitative feel for the distortion can be derived from the tilt and twist angles.[3g] For a planar amidic unit lying in the X–Z plane with N–C along the *x*-axis, the twist and tilt angles are, respectively, defined as the rotation angle of the N lone pair out of optimum conjugation with the C=O π-system (e.g., rotation about the *x*-axis) and the tilt of the lone pair away from the *y*-axis. Lone-pair position is defined by a perpendicular drawn through N, normal to the plane defined by the three attached C's.

Table IV. Activation Parameters for the Hydrolysis of **1a–d** and **3a** in Aqueous Acid and Base (μ = 1.0 (KCl))[a]

	acid		base	
amide	$\Delta H^{\ddagger}$, kcal/mol	$\Delta S^{\ddagger}$, eu	$\Delta H^{\ddagger}$, kcal/mol	$\Delta S^{\ddagger}$, eu
1a	10.26 ± 0.64[b]	−21.5 ± 2.4	7.58 ± 0.73	−22.0 ± 2.7
1b	6.60 ± 0.47[c]	−28.3 ± 1.8[c]	7.20 ± 1.22	−26.3 ± 4.7
1c	6.25 ± 0.45[c]	−31.6 ± 1.7[c]	9.08 ± 0.36	−23.1 ± 1.4
	8.01 ± 0.51[d]	−27.9 ± 2.0[d]		
1d	15.96 ± 0.08[e]	−22.5 ± 0.3[e]	13.20 ± 0.15	−29.2 ± 0.7
3a	19.7 ± 0.4[d]	−22.8 ± 0.8[d]	11.9 ± 0.2	−39.8 ± 0.5

[a] Five to six temperatures. Activation parameters calculated according to Eyring equation from second order rate constants. Error limits computed according to the method described in: Wiberg, K. B. *Physical Organic Chemistry*, 2nd ed.; Wiley: New York, 1966; p 379. [b] Data of ref 3a reevaluated according to Eyring equation from pseudo-first-order rate constants at pH 3.2. Three temperatures. [c] pH 2.0. [d] pH 0.0. [e] pH 1.5.

to the form given in eq 3. For the remaining least reactive amides (**1d**, **3a**), which show no evidence for a kinetic pK_a' at low pH ($K_a' \gg [H^+]$), the kinetic expression further simplifies into $k_{hyd} = k_1[H^+]/K_a' + k_3[OH^-]$.

$$k_{hyd} = \frac{k_1[H^+]}{K_a' + [H^+]} + k_3[OH^-] \qquad (3)$$

Given in Table III are the rate and dissociation constant values derived by fitting of the k_{hyd} vs $[H^+]$ data for the various amides to their respective equations, the quoted errors being obtained from the standard deviations of the fit parameters. As can be judged from comparison of the constants in the fourth and fifth columns of Table III, there is a marked activation of at least 7 orders of magnitude in k_3 and 11 orders of magnitude in k_1/K_a' in passing from the least to the most distorted anilide.[12] The comparison of the acid terms indicates that the apparent rate acceleration arises from two components, namely the accelerated attack of H_2O on the protonated forms of the distorted amides and the increasing pK_a' of their conjugate acid forms. As judged from k_1, the most heavily distorted amide (**1a**) is less reactive toward H_2O attack on the fully protonated form than are less distorted **1b,c**.

Also included in Table III are k_3 rate constants determined in D_2O/OD^- media. From these can be derived the kinetic solvent isotope effects for OL^- attack $k_3^{OH^-}/k_3^{OD^-}$; **1a**, 1.10 ± 0.10; **1b**, 0.97 ± 0.04; **1c**, 1.31 ± 0.15; **1d**, 0.97 ± 0.11.

Finally, given in Table IV are the activation parameters for the hydrolysis of **1a–d** and **3a** in H_2O (μ = 1.0, KCl). For **1b–d** and **3a** the pseudo-first-order rate constants at five to six temperatures at a given $[OH^-]$ or $[H_3O^+]$ were converted to second-order ones and plotted in the usual way according to the Eyring equation[13] to yield the $\Delta H^{\ddagger}$ and $\Delta S^{\ddagger}$ values. For **1a**, that protocol was used in base, but in acid at pH 3.2 where the reaction is pH independent, the pseudo-first-order rate constants at three temperatures[3a] were fit to the appropriate form of the Eyring equation. We were forced to use that pH, since in the pH 4–6 domain where the hydrolysis is first order in $[H_3O^+]$ extensive buffer catalysis with acetate and formate is observed, which complicates the analysis.

Effects of Acetate Buffer on the Hydrolysis of 1b,c in H_2O and D_2O, T = 25 °C (μ = 1.0, KCl). Marked buffer catalysis of the hydrolysis of **1b** and **1c** is observed in both H_2O and D_2O media from pH 4 to 6. At each pH (pD) value, pseudo-first-order rate constants were evaluated in duplicate at $[acetate]_{total}$ varying between 0.05 and 0.2 M. The buffer component, $k_{OAc}(app)$, was evaluated as the slope of the plots of k_{hyd} vs $[acetate]_{total}$, with the intercept being the pseudo-first-order rate constant for acid hydrolysis at a given L_3O^+.

(12) The deemed rate acceleration depends upon the comparison material. Probably 2,*N*-dimethylacetanilide (3: X = H, Y = CH_3) is a more appropriate reference, but no detectable hydrolysis of this was observed after 50 h, T = 100 °C, 0.2 M OD^-/D_2O.

(13) Glastone, S.; Laidler, K. J.; Eyring, H. *The Theory of Rate Processes*; McGraw-Hill: New York, 1941.

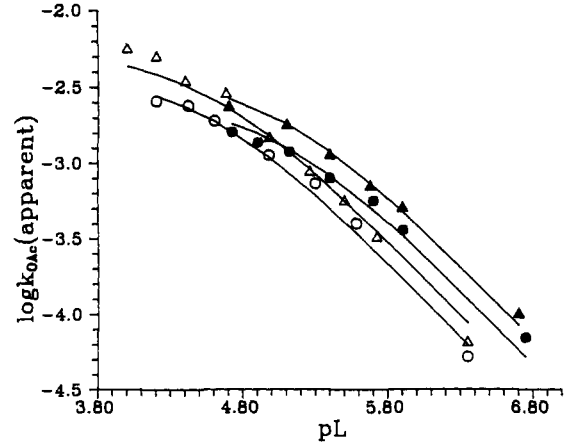

Figure 4. Plots of log k_{OAc}(app) vs pL for the hydrolysis of **1b** (△) and **1c** (○) in H_2O (open symbols) and D_2O (closed symbols) media (T = 25 °C, μ = 1.0 (KCl)). Line drawn through the data is that computed by a nonlinear least-squares fit to the second term in eq 5.

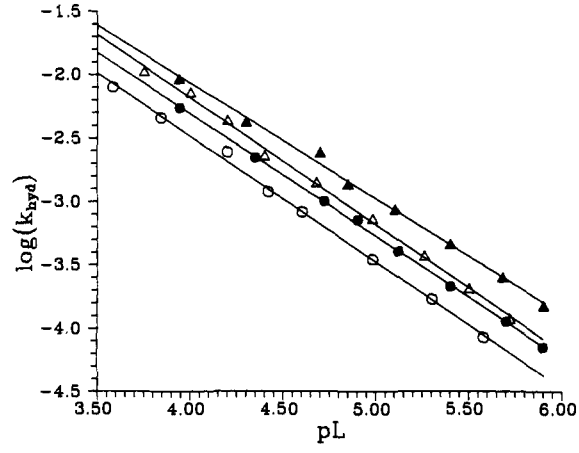

Figure 5. Plot of log k_{hyd} vs pL for **1b** (△) and **1c** (○) derived from the intercepts of plots of k_{hyd} vs $[acetate]_{total}$ at various pL values in H_2O (open symbols) and D_2O (closed symbols) media (T = 25.0 °C, μ = 1.0 (KCl)).

Shown in Figure 4 are the log k_{OAc}(app) vs pL plots for acetate catalysis of the hydrolysis of **1b** and **1c**, respectively, in both H_2O and D_2O. In Figure 5 are shown the plots of the intercepts (extrapolated to zero $[acetate]_{total}$) vs pL for **1b** and **1c**, respectively, in both H_2O and D_2O. The feature of note in Figure 4 is the plateauing of the log k_{OAc}(app) values below the pK_a for LOAc and the greater reactivity in H_2O than D_2O.

The data shown in the latter two figures suggests the role of acetate is to act as a general base in delivering L_2O to A-L^+ in accordance with the mechanism outlined in eq 4 from which can be derived the kinetic expression given in eq 5, where K_a and K_a' are the acid dissociation constants of LOAc and A-L^+, respectively.

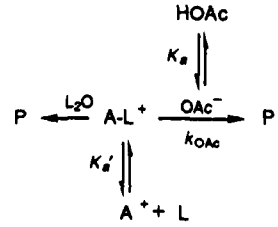

(4)

$$k_{hyd} = \frac{k_1[L^+]}{K_a'} + \frac{k_{OAc}}{K_a'}\left(\frac{K_a[L^+]}{[L^+] + K_a}\right)[acetate]_{total} \qquad (5)$$

Nonlinear least-squares fitting of the data used to construct Figure 4 to the second term in eq 5 yields the constants for **1b** and **1c** given in Table V. In order to evaluate the k_{OAc}/K_a' constant, the LOAc dissociation constant (K_a) was fixed at the

Table V. Rate Constant Data for the Effect of Acetate on the Hydrolysis of **1b** and **1c** in H_2O and D_2O (T = 25.0 °C, μ = 1.0 (KCl))

amide	k_{OAc}/K_a'[a] H_2O	k_{OAc}/K_a'[a] D_2O	$(k_{OAc}/K_a')^{H_2O}/(k_{OAc}/K_a')^{D_2O}$	$(k_1/K_a')^{H_2O}/(k_1/K_a')^{D_2O}$[b]
1c	143 ± 7	298 ± 18	0.48 ± 0.08	0.63 ± 0.05
1b	197 ± 11	429 ± 45	0.46 ± 0.12	0.62 ± 0.03

[a] Evaluated from nonlinear least-squares fitting of the data used to construct Figure 4 to the second term of eq 5. K_a fixed at the apparent values for LOAc (μ = 1.0); $pK_a(H_2O)$ = 4.55; $pK_a(D_2O)$ = 5.05. Errors quoted from the NLLSQ fits. [b] Evaluated at pL = 4.8 from data used to construct Figure 5.

apparent values corrected[8] to an ionic strength of 1.0 ($K_a(H_2O) = 2.818 \times 10^{-5}$; $K_a(D_2O) = 8.913 \times 10^{-6}$). Of note from the data in Table V is the fact that k_{OAc}/K_a' is larger in D_2O than H_2O (an apparent inverse solvent kinetic isotope effect (KIE) once the effect of L_2O on the pK_a of LOAc is taken into account (vide infra).

Also given in Table V are the solvent KIE values on k_1/K_a' derived at pL 4.8 from the data shown in Figure 5. Of note here is the apparent inverse solvent isotope effect arising from a kinetic isotope effect for H_2O attack superimposed on an equilibrium isotope effect on K_a'.

Discussion

(a) Structure of 1b–d and 3b. The nature of the bicyclic ring system in **1a–d** produces a substitutionally similar set of anilides in which there is a continuous variation in the degree of distortion about the amide linkage. As determined from the X-ray diffraction studies, the distortion manifests itself in a lengthening of the N—C(O) bond, a slight shortening of the C=O bond, and a twisting about the N—C(O) unit with attendant pyramidalization of the N. Since there appear to be no unusually close contacts within the unit cell of these amides, crystal packing forces are unlikely to be a major factor in determining the structure. Although we do not have at present crystals of **1a** that are of sufficient quality for detailed X-ray diffraction studies, its rigidity demands it to be the most orthogonal of the series.[9]

The experimentally determined alteration in the amidic bond lengths and hybridizations that accompany rotation about the N—C(O) bond can be compared with the situation predicted theoretically[14] for formamide in its planar (**7a**) and two orthogonal conformers (**7b,c**).

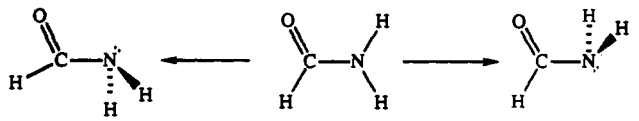

7b **7a** **7c**

ΔE(kcal/mol) 18.67 0.0 15.98

Wiberg and Laidig[14] have calculated that in passing from **7a** to orthogonal formamide **7b** (which is configurationally similar to anilides **1a–d**) there is a lengthening of the N—C(O) bond by 0.075 Å and a shortening of the C=O bond of ~0.015 Å as well as a hybridization change at N to sp^3 from sp^2. The computed barrier to rotation (through **7c**) closely approximates the experimental one.[15] In addition, charge analysis using the atomic population analysis formulated by Bader[16a] indicates that, in contrast to the resonance model, the computed electron population

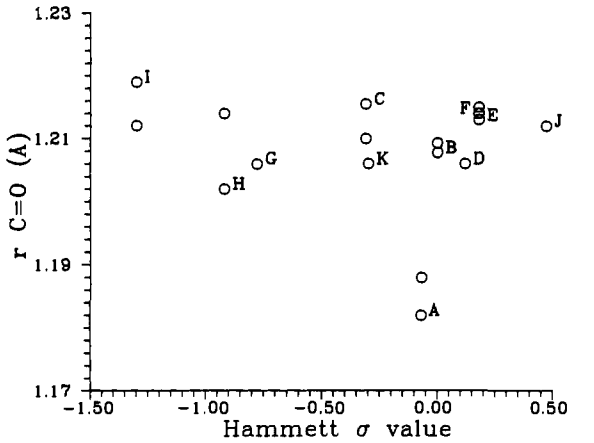

Figure 6. Plot of gas-phase C=O bond length vs Hammett σ value of substituent X for H(C=O)X derivatives. For electron donors, σ^+ is used; for electron withdrawers, σ is used. Key (X): A (F), V (H), C (CH_3), D (CH_2Cl), E ($CH{=}CH_2$), F ($C{\equiv}CH$), G (OCH_3), H (OH), I (NH_2), J (CHO), K ($(CH_3)_2CH$). Where two data are given for a single letter, these were determined from independent analyses.

at N in **7a** is larger than in **7b,c** while the population at O in each is similar. Also, the electron density at C in **7b,c** is larger than in **7a** so that passing from the orthogonal to planar forms involves a net charge transfer of C → N and not N → O as would be predicted by the resonance model. Wiberg and Laidig[14] and Bader et al.[16b] conclude that amidic resonance as is customarily invoked to involve N → O charge transfer does not exist and the structural properties stem from N rehybridization that accompanies rotation about the N—C(O) bond.

The calculated relative insensitivity of the C=O bond length in formamide to rotation about the C—N bond[14] invites comparison with experimental C=O lengths for amides that have varying degrees of conjugative ability. To the extent that the bond length is related to the stretching force constant, conjugation is anticipated to reduce the C=O force constant and lengthen the bond. Because the C=O force constant is inherently larger than the C—N force constant,[14b] it is to be expected that structural or electronic perturbations might lead to a larger variation in the C—N than C=O bond length. What the anticipated change in C=O bond length should be as a function of decreased conjugating ability of the amide N is difficult to assess; however, one does anticipate some consistent shortening. Comparison of the gas-phase electron diffraction and/or microwave data for amides **8–11**[17-20] indicates the C=O bond length is rather insensitive to

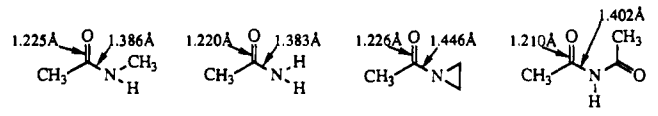

8[17] **9**[18] **10**[19] **11**[20]

the anticipated poorer N lone pair donating ability in **10** or **11** relative to that in **8** or **9**. The C-N bond length changes are somewhat greater, but even in the case of **11** where the anticipated conjugation of N to each of its attached C=O units is roughly half of that expected in **8** or **9**, the C-N bond length is only slightly perturbed.

The above data demand that we ask how large a C=O variation might be anticipated for a series of acyl derivatives (R(C=O)X) in which the group X changes markedly in its electron-donating or -withdrawing ability. Shown in Figure 6 is a plot of the gas-phase experimentally determined C=O bond lengths[21] for

(14) (a) Wiberg, K. B.; Laidig, K. E. *J. Am. Chem. Soc.* **1987**, *109*, 5935. (b) Wiberg, K. B.; Breneman, C. M. To be published. We thank Professor Wiberg for a preliminary draft of this manuscript.

(15) For microwave structural studies of formamide, see: (a) Hirota, E.; Sugisaki, R.; Nielsen, C. J.; Sorensen, G. O. *J. Mol. Spectrosc.* **1974**, *49*, 251. (b) Costain, C. C.; Dowling, J. M. *J. Chem. Phys.* **1960**, *32*, 158.

(16) (a) Bader, R. F. W.; Nguyen-Dang, T. T. *Adv. Quantum Chem.* **1981**, *14*, 63. (b) Bader, R. F. W.; Cheeseman, J. R.; Laidig, K. E.; Wiberg, K. B.; Breneman, C. M. *J. Am. Chem. Soc.* **1990**, *112*, 6530. We thank Professor Bader for a copy of this manuscript prior to publication.

(17) Kitano, M.; Fukuyama, T.; Kuchitsu, K. *Bull. Chem. Soc. Jpn.* **1973**, *46*, 384.

(18) Kitano, M.; Kuchitsu, K. *Bull. Chem. Soc. Jpn.* **1973**, *46*, 3048.

(19) Tarasenko, N. A.; Avakyan, V. G.; Belik, A. V. *Zh. Strukt. Khim.* **1978**, *19*, 541; *Russ. J. Struct. Chem. (Engl. Transl.)* **1978**, *19*, 470.

(20) Gallaher, K. L.; Bauer, S. H. *J. Chem. Soc., Faraday Trans. 2* **1975**, 1423.

formyl derivatives against the σ^+ or σ value for the substituent (for electron donors, σ^+ is used; for electron withdrawers, σ is used).[22] With the exception of the acid halide (HC(O)F) all the C=O bond lengths lie in a narrow range from 1.20 to 1.23 Å despite the large variation in the σ^+ or σ value of the substituents. In examination of 16 H(C=O)X derivatives and 24 YCH_2(C=O)X derivatives,[21] only acid halides, formic anhydride,[23] acetic anhydride,[24] and fluoromethyl formate[25] have gas-phase C=O bond lengths less than the above range, and these lie between 1.18 and 1.20 Å. Nevertheless, since there is little regular change in passing from the most π-electron-donating X (NH_2,OR) to the most electron-withdrawing ones (X = CHO, CH=CH_2, CF_3) it is apparent that no predictable relationship between C=O bond length and the electronic nature of X exists.

It might be argued that the C=O bond in acyl derivatives is so heavily polarized (C^+-O^-)[14] that its length becomes insensitive to the nature of X. If so, then a less polarized C=C double bond in H_2C=CHX derivatives may exhibit a greater variation in length as a function of different electron-withdrawing or -donating substituents. However, the gas-phase structural data[21] for a series of XCH=CH_2 indicate that even the C=C double bond is insensitive to the electronic nature of X as measured by σ_X.[22]

On the basis of the above data, one is forced to conclude that little structural evidence exists to support the notion that a C=O or C=C bond length should respond in a particular way to substituents capable of donating or withdrawing electrons by resonance. Of course, the substitution markedly alters the chemical reactivity of the π-bond, and this may be a consequence of putative resonance. The experimental structural data for **1b–d** and **3b** compare favorably with that predicted[14] for planar and orthogonal formamide, but they provide no information concerning the changes in electronic distribution that accompany N—C(O) bond rotation. Although the theoretical analysis concerning the deficiency of the resonance model in explaining the charge distributions in formamide is intriguing, experimental verification is conspicuously sparce. At present, it would be capricious to discard such a historically useful device as amidic resonance unless satisfactory altenative explanations are found for all of the properties of amides that are currently rationalized within that framework.[26]

(b) Hydrolysis of 1a–d and 3a. Whether one need invoke resonance or not, distortion of an amide in a way that would remove resonance[1-3,27] accelerates the rate of hydrolysis in both acid and base (Table III). For the anilides in the table, the rate enhancement for acid-catalyzed hydrolysis as judged by k_1/K_a' is roughly 11 orders of magnitude and is controlled not only by the rate constant for H_2O attack on A-H^+ but also by how extensively the amide is protonated at a given [H_3O^+]. The most distorted amides (**1a–c**) show evidence of a kinetic pK_a for A-H^+ that has been interpreted as arising from H_2O attack on an N-protonated form.[3a,f] The greater the molecular distortion, the higher the kinetic pK_a so that the distorted amides are more extensively protonated at a given pH than are the undistorted ones. A high pK_a (A-H^+) is not the sole reason for accelerated hydrolysis in acid, since when fully protonated **1a** is less susceptible toward H_2O attack (as judged from k_1) than is **1b** or **1c**.[27]

In basic media, all these anilides hydrolyze by mechanisms that are first order in [OH^-]. Roughly 7 orders of magnitude in rate separates **1a** from **3a**. In an earlier study[3a] we failed to detect any C=^{18}O carbonyl exchange in base, which was interpreted in terms of a mechanism in which the rate-limiting step is that involving attack of OH^- on **1a,b** as in eq 6. However, such

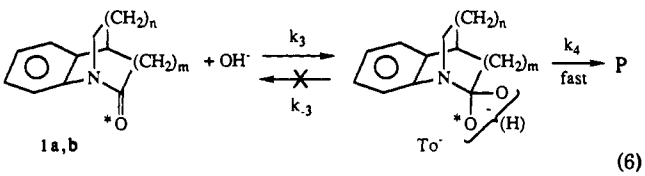

(6)

^{18}O-exchange data in the case of these bicyclic anilides must be interpreted cautiously since the bicyclic structure does not allow the two oxygens to To$^-$ to be symmetrized even if rapid O–*O proton transfer occurs. Nevertheless, due to the inherent ground-state destabilization in the bicyclic series, the slow step in the hydrolysis is likely k_3 (eq 6). Anilides **1a–d** exhibit solvent KIE's for OL^- attack ranging from ~1.0 to 1.3 (no ordering in the series), which is consistent with a rate-limiting attack step. For toluamides **12a,b**[28] and **12c**,[29] where the rate-limiting step for

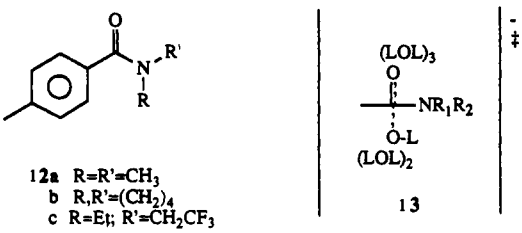

12a R=R'=CH_3
b R,R'=$(CH_2)_4$
c R=Et; R'=CH_2CF_3

13

hydrolysis (**12a,b**) and ^{18}O exchange in recovered amide (**12c**) is k_3, the solvent KIE's for OL^- attack are close to unity, the respective values being 0.90 ± 0.15, 0.92 ± 0.05, and 0.90 ± 0.08. Admittedly, **12a–c** are structurally different from anilides **1a–d**, and despite the expectation that OD^- in D_2O is anticipated to be a better nucleophile than OH^- in H_2O,[30] the consistency of the anilide and toluamide results suggests a commonality of mechanism. In the latter toluamide case, the near-unit value for the SKIE was attributed[28,29] to the process shown in **13** where, at the transition state, desolvation of the attacking lyoxide is compensated by solvation of the developing alkoxy anion.

It has been reported[31] that the solvent KIE for OL^- attack on **3a** is k_{OH^-}/k_{OD^-} = 1.16 in L_2O at 76.7 °C in the presence of 1 M NaOL. On the basis of that isotope effect and those for other para-substituted *N*-methylacetanilides, Gani and Viout[31] have suggested that the rate-limiting step for OL^- attack on **3a** is the water-assisted decomposition of the corresponding anionic tetrahedral intermediate. Such a mechanism implies that an ^{18}O isotopically substituted **3a** should show large amounts of ^{18}O exchange accompanying its hydrolysis. Accordingly, Des-

(21) All C=O or C=C bond lengths are determined by electron diffraction or microwave techniques and can be found in: (a) Hirota, E.; Kuchitsu, K. *Landolt-Börnstein New Series II* **1976**, *7*, 108–392. (b) Hirota, E.; Iijima, T.; Kuchitsu, K. *Landolt-Börnstein New Series II* **1987**, *15*, 137–608.

(22) Given the relative insensitivity of the C=O and C=C bond lengths to the substituent, it is a moot point as to which is the appropriate σ to use for the correlation in Figure 6.

(23) Vaccani, S.; Roos, U.; Bauder, A.; Günthard, H. H. *Chem. Phys.* **1977**, *19*, 51.

(24) Vledder, H. J.; Mijlhoff, F. C.; Leyte, J. C.; Romers, C. *J. Mol. Struct.* **1971**, *7*, 421.

(25) Lopata, A. D.; Kuczkowski, R. L. *J. Am. Chem. Soc.* **1981**, *103*, 3304.

(26) While we remain presently uncommitted to whether amidic resonance exists or not, we have provided an alternative rationale for the accelerated hydrolysis of distorted amides;[3g] however, even that rationale is not inconsistent with a resonance model. Ongoing work in these laboratories addresses the adequacy of the resonance model in explaining the physicochemical properties of these and other amides.

(27) This phenomenon appears to be analogous to the effects reported by Fersht and Jencks[27a] and Williams[27b] who studied the relationship between the rate constants for H_2O attack and leaving group pK_a in a series of *N*-acylpyridinium and *N*-acetyltrialkylammonium ions, respectively. In the latter study,[27b] a β_{lg} of –0.5 was determined so that the higher the pK_a of the conjugate acid of the leaving group, the less reactive toward water attack was the attached *N*-acyl group. In the present study, the pK_a of the anilinium ions of the corresponding hydrolysed amino acids is not expected to be markedly different. However, due to the different distortion inherent in the bicyclic amides, the kinetic pK_a of their N-protonated forms varies. In the series **1a**, **1c**, and **1b**, a rather poor $\beta_{(NH^+)}$ of –0.27 ± 0.21 obtains. Although we are convinced that the thermodynamic site of protonation for each is N, the poorness of the fit could result from differences in the extent of involvement of H_2O attack on N protonated and O protonated forms. (a) Fersht, A. R.; Jencks, W. P. *J. Am. Chem. Soc.* **1970**, *92*, 5432. (b) Williams, A. *Ibid.* **1976**, *98*, 5645.

(28) Slebocka-Tilk, H.; Bennet, A. J.; Keillor, J.; Brown, R. S.; Guthrie, J. P. *J. Am. Chem. Soc.* **1990**, *112*, 8507.

(29) Slebocka-Tilk, H.; Bennet, A. J.; Hogg, H. J.; Brown, R. S. *J. Am. Chem. Soc.* **1991**, *113*, 1288.

(30) See Alvarez, F. J.; Schowen, R. L. In *Isotopes in Organic Chemistry*; Buncel, E., Lee, C. C., Eds.; Elsevier: Amsterdam, 1987; Vol. 7, pp 1–60.

(31) Gani, V.; Viout, P. *Tetrahedron* **1976**, *32*, 1669.

longchamps et al.[32] have reported that considerable ^{18}O exchange does accompany the base hydrolysis of **3a** at temperatures between 27 and 90 °C. We have repeated[33] the exchange experiment with ~50% ^{18}O-labeled **3a** at 74.0 ± 0.5 °C with the following time (percent ^{18}O content) data for amide recovered from the hydrolytic medium (1.077 M OH^-): 0 min, 48.42 ± 0.40; 12 min, 42.13 ± 0.32; 24 min, 36.39 ± 0.36; 48 min, 28.07 ± 0.45. Under these conditions, $k_{hyd} = 4.81 \times 10^{-4}$ s^{-1} while $k_{ex} = 1.89 \times 10^{-4}$ s^{-1} so that $k_{ex}/k_{hyd} = k_{-3}/2k_4 = 0.39$ (rate constants defined analogously to the process defined in eq 6). From these data, it can be concluded that the reported solvent KIE data of Gani and Viout[31] for **3a** is not determined by a single kinetic step, but rather by the virtual transition state that corresponds to the partitioning of the anionic tetrahedral intermediate.[34] Therefore, the data for **3a** cannot be compared directly to the SKIE data for **1a–d**, which pertain to the k_3 step.

(c) Activation Parameters for the Hydrolysis of 1a–d and 3a. In order to more fully understand the factors controlling the changes in rate produced by distortion, we have obtained the activation parameters given in Table IV. In base, as expected for the bicyclic anilides, the largest $\Delta G^{\ddagger}_{25}$ obtains for least distorted **1d**. The bulk of the activation produced by distortion in passing from **1d** through the series to **1a** appears as a reduction in the $\Delta H^{\ddagger}$. Additionally, a smaller component of ~20% of the $\Delta G^{\ddagger}_{25}$ results from a less (−) $\Delta S^{\ddagger}$. From the previous section, these activation parameters refer to the isolated kinetic step, k_3 (eq 6), involving OH^- attack on **1**. Due to the increasing ground-state distortion of the anilide in passing from **1d** → **1a**, the changes in the activation parameters can be explained by Hammond postulate,[35] arguments that imply the transition state becomes increasingly earlier with less OH–**1** bond making, and less restriction of solvent. For OH^- attack on **3a**, which was previously (vide supra) shown not to be uniquely rate limiting, the corresponding activation parameters given in Table V refer to the virtual transition state leading to and away from To$^-$ and so cannot be directly compared to those of **1**.

In acid, where the reactions are in the domain that is first order in $[H_3O^+]$ and so can be compared in terms of k_1/K_a', the apparent activation parameters refer to the composite of those of the rate constant for H_2O attack and those involved in determining K_a'. Only in the case of **1a**, where at pH 3.2 the amide is fully protonated, do the activation parameters refer to H_2O attack on **1a**-H^+ (k_1). For the remaining anilides, apparently distortion causes a marked reduction in the apparent $\Delta H^{\ddagger}$ in passing from **3a** to **1b**, but there appears to be no general trend in $\Delta S^{\ddagger}$, probably because of the differential entropic terms in K_a'. From the case of **1c** in which the activation parameters were evaluated at pH 2 and 0 (above and below the pK_a (0.56) of **1c**-H^+, respectively), a weak conclusion can be drawn in terms of the relative activation parameters on k_1 and k_1/K_a'. At pH 0, where **1c**-H^+ comprises the majority of the species in solution, the $\Delta H^{\ddagger}$ and $\Delta S^{\ddagger}$ refer principally to the attack of H_2O on the protonated amide. Here, the higher $\Delta H^{\ddagger}$ and less (−) $\Delta S^{\ddagger}$ than observed at pH 2 obtains from the fact that the ground state is **1c**-H^+ (lower in energy than **1c**) and has restricted waters of solvation that are in place prior to the attainment of the transition state. That situation appears to hold as well for **1a**-H^+ at pH 3.2.

(d) Effect of Acetate on the Hydrolysis of 1b,c in H_2O and D_2O. The analysis (according to the mechanism given in eq 4) of the hydrolysis k_{obsd} vs $[acetate]_{total}$ plots at various pL values in H_2O and D_2O allows one to derive the constants given in Table V. The appearance of the log k_{OAc}(app) vs pL plots shown in Figure 4 indicates a plateauing below the pK_a of LOAc, which implies that the pL-independent region results from some acetate-dependent process for which the transition state is formally neutral. This could be represented as either a general-acid-catalyzed process (A + L_2O + LOAc) or its more likely kinetic equivalent, a specific-acid/general-base-catalyzed process (A–L^+ + L_2O + OAc^-). Importantly, when fully plateaued (at low pH), the catalyzed reaction in H_2O is faster than in D_2O for both **1b** and **1c**. In an earlier study[3a] we have shown that in CD_3CN OAc^- is capable of nucleophilically attacking **1b**-H^+ (eq 7) to yield an open anhydride (**14**). Similarly, the monoanions of several di-

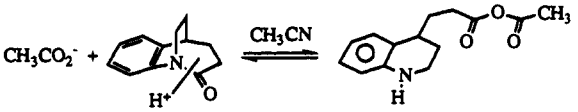

1b-H^+ **14** (7)

carboxylic acids (maleic, succinic, glutaric, *cis*-cyclopropane-1,2-dicarboxylic) are also capable of acting as nucleophiles toward **1b**-H^+.[3e] However, **14** has also been shown[3e] to rapidly re-form **1b** + OAc^- when in aqueous acetate-buffered media so that the accelerated hydrolysis observed in acetate buffers in the present study probably does not result from nucleophilic attack.

The currently favored mechanism is a specific-acid/general-base process shown in eq 8 that leads to **15a,b**. The observed solvent KIE for such a process would be comprised of three individual isotope effects, namely the two equilibrium isotope effects on the K_a' of **1**-L^+ and K_a of LOAc, as well as the kinetic isotope effect involved in the catalyzed delivery of LOL to **1**-L^+. To assist in

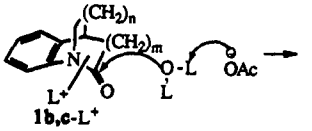

1b,c-L^+

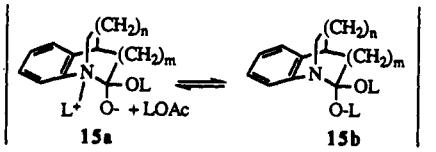

15a **15b** (8)

the dissection of the observed KIE into its components, we have used the known shift of the thermodynamic pK_a of LOAc in passing from H_2O to D_2O of +0.5 unit[7] (corrected to $\mu = 1.0$;[8] p$K_a(H_2O)$ = 4.55, p$K_a(D_2O)$ = 5.05) to evaluate the k_{OAc}/K_a' values in H_2O and D_2O given in Table V. Since it is generally observed that oxygen and nitrogen acids are stronger by a factor of ~3 in H_2O than in D_2O[36] (since D_3O^+ is a stronger acid in D_2O than is H_3O^+ in H_2O), one might anticipate that K_a' should be a factor of ~3 larger in H_2O than D_2O. Thus, the change from H_2O to D_2O will lead to a counterbalancing of the two kinetically competent forms of **1**-L^+ and OAc^- in eq 8 since the increase in [**1**-L^+] is compensated by an equivalent decrease in [OAc^-]. On the basis of the above, the computed $(k_{OAc}/K_a')^{H_2O}/(k_{OAc}/K_a')^{D_2O}$ of 0.46 and 0.48, respectively, for **1b** and **1c**, when modified by the anticipated K_a' (H_2O) ≃ 3K_a'(D_2O) yields a small normal KIE on the k_{OAc} terms for acetate promoted delivery of LOL to **1b** and **1c** of 1.38 and 1.44, respectively, consistent with the mechanism given in eqs 4 and 8.

As shown in Figure 5 and given in Table V as $(k_1/K_a')^{H_2O}/(k_1/K_a')^{D_2O}$, there is an apparent inverse isotope effect for uncatalyzed attack of L_2O on **1**-L^+ of ~0.62 for each of **1b** and **1c**. This process is analogous to that described above for the acetate effect. Using a similar estimate of the influence of the H_2O to D_2O change on the K_a', a normal primary isotope effect of 1.86 can be computed for L_2O attack on **1**-L^+ ($k_1^{H_2O} = 3 \times 0.62 k_1^{D_2O}$).

(32) Deslongchamps, P.; Gerval, P.; Cheriyan, U. O.; Guida, A.; Taillefer, R. J. *Nouv. J. Chim.* **1978**, *2*, 631.

(33) Although the Deslongchamps' study[32] provided adequate evidence of ^{18}O exchange for **3a**, insufficient data were reported concerning the experimental protocol to allow a k_{ex} value to be determined accurately.

(34) It is possible that the SKIE data reported for **3a**[31] refer to a more complicated situation than a reversible addition to produce To$^-$ where the k_{-3} and k_4 steps are nearly isoenergetic. Under comparable conditions (0.2 M OD^-/D_2O, 100 °C) we have observed that *N*,2-dimethylacetanilide undergoes complete exchange of the $C(O)CH_3$ group within 30 min. Bennet, A. J.; Brown, R. S. Unpublished results. A similar exchange should obtain with **3a** in OD^-/D_2O, so that the actual SKIE refers to the reversible attack of OD^- on $C(O)CH_xD_{3-x}$ (x = 1–3).

(35) (a) Hammond, G. S. *J. Am. Chem. Soc.* **1955**, *77*, 3608. (b) Farcasiu, D. *J. Chem. Educ.* **1975**, *52*, 76.

(36) Gold, V. *Adv. Phys. Org. Chem.* **1969**, *7*, 259.

This isotope effect is consistent with the process shown in eq 9, wherein L_2O acts as a general base in delivering a second L_2O to the protonated amide to yield **15a,b**.[37]

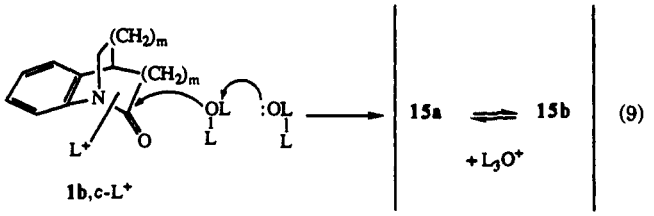

(9)

Conclusions

(1) Progressive distortion of the anilides **3b** → **1d** → **1b,c** leads to a lengthening of the N—C(O) bond with only a small shortening of the C=O bond and a rehybridization of the N from sp^2 to sp^3 that accompanies rotation around the C—N bond. The insensitivity of the C=O bond length to the distortion is at first surprising but appears normal when compared with the lengths of C=O bonds in two series of RC(O)X derivatives where group X varies markedly in its ability to donate or withdraw electrons.

(2) Progressive distortion of the anilides leads to marked acceleration of the acid- and base-promoted hydrolyses. The respective domains are first order in $[H_3O^+]$ and $[OH^-]$, but there is a progressive increase in the kinetic pK_a of the protonated amide with distortion that arises from a shift from O to N protonation. The activation parameters indicate that the bulk of the rate increase in base that accompanies distortion results from a reduction in $\Delta H^{\ddagger}$ (13.2 kcal/mol (**1d**) to 7.58 kcal/mol (**1a**)) with an increase in the $\Delta S^{\ddagger}$ (−29.2 eu (**1d**) to −22.0 eu (**1a**)). In H_3O^+, analysis of the activation parameters is less straightforward since they pertain to a ratio of a kinetic and an equilibrium term (k_1/K_a').

(3) Solvent kinetic isotope data establish that both acetate and solvent act as general bases to deliver L_2O to the protonated forms of **1b** and **1c**.

Acknowledgment. We gratefully acknowledge the financial support of the University of Alberta and the Natural Sciences and Engineering Research Council of Canada. In addition, were are grateful to Dr. X. Huang for obtaining crystals of **1d** suitable for X-ray crystallographic study. Finally, we are indebted to Professor K. B. Wiberg for a preliminary draft of a manuscript.[14b]

Supplementary Material Available: Synthetic procedure for **3b**, tables of atomic coordinates and isotropic parameters of **1d** and **3b**, data collection techniques and structure solution and refinement details, tables of interatomic bond lengths and angles and torsional angles, tables of hydrogen atom coordinates and root-mean-square amplitudes, and figures giving labeling schemes for molecules A and B and the packing motif of A and B (19 pages); listing of structure factor amplitudes (19 pages). Ordering information is given on any current masthead page.

(37) The KIE can also be evaluated by the fractionation factor analyses.[38] Thus, for the acetate-promoted delivery of L_2O, if the ground state in the plateau region consists of **1b,c** + LOAc + L_2O and the transition state is as given in eq 8, the KIE is determined by a single proton in flight having a fractionation factor of 0.65–0.7 (KIE = k_{OAc}^{H}/k_{OAc}^{D} = 1.54–1.42). For water-promoted delivery of L_2O, if the ground state consists of **1b,c** + L_3O^+ + L_2O, the KIE = $(k_1/K_a')^{H_2O}/(k_1/K_a')^{D_2O}$ = 0.66 is determined by a single proton in flight (0.5) and the fractionation factor for L_3O^+ (0.69[3]). That the fractionation factors for a proton in flight from acetate + L_2O, and L_2O: + L_2O are slightly different is attributable to an earlier TS for the acetate promoted reaction.

(38) (a) Schowen, R. L. In *Isotope Effects on Enzyme Catalyzed Reactions*; Cleland, W. W., O'Leary, M. H., Northrup, D. B., Eds.; University Park Press: Baltimore, MD, 1977. (b) Schowen, R. L. *Prog. Phys. Org. Chem.* **1972**, *9*, 275.

Terpenoids to Terpenoids: Enantioselective Construction of 5,6-, 5,7-, and 5,8-Fused Bicyclic Systems. Application to the Total Synthesis of Isodaucane Sesquiterpenes and Dolastane Diterpenes

Goverdhan Mehta,* Nacharaju Krishnamurthy, and Srinivas Rao Karra

Contribution from the School of Chemistry, University of Hyderabad, Hyderabad 500 134, India.
Received December 4, 1990

Abstract: The prevalence of a C_{12} common core (**10**) in C_{15}–C_{30} terpenoids has been recognized. Construction of two "chirons" ((−)-**11** and (−)-**12a,b**), corresponding to **10**, from abundantly available (*R*)-(+)-limonene has been achieved through diastereoselective [3s.3s] sigmatropic processes **16** → **11** and **19** → **12**, respectively. Chirons **11** and **12** have been successfully annulated to bicyclic hydrindanones **21**, **23**, and **30**, hydrazulenoids **31**–**33**, and 5,8-fused system **42** through methodologies that are short and practical. Thus, these enantiomerically pure bicyclics are available as advanced building blocks for higher terpene synthesis. One of the hydrazulenoids ((−)-**31**) has been elaborated to isodaucane sesquiterpenes (+)-aphanamol I (**2**) and (+)-2-oxoisodauc-5-en-12-al (**46**) through a novel restructuring protocol (**31** → **50**). The stereo- and enantioselective synthesis reported here has established the absolute stereochemistry of isodaucane sesquiterpenes. The hydrazulenoid (−)-**31** has also been deployed for the first enantioselective synthesis of oxygenated dolastane diterpenes (+)-isoamijiol (**63**) and (+)-dolasta-1(15),7,9-trien-14-ol (**64**). The key step in this venture was the stereoselective annulation of a six-membered ring through radical-induced alkyne–carbonyl cyclization (**67** → **68**).

The overwhelming accent on carbohydrates as "chirons" for natural products synthesis, during the past decade, has somewhat marginalized the importance of abundantly available terpenes as building blocks for chiral synthesis.[1,2] This has come about despite the fact that many terpenes are cheap, readily accessible, and endowed with only one or two chiral centers with modest func-

(1) Hanessian, S. *Total Synthesis of Natural Products: The Chiron Approach*; Pergammon Press: Oxford, 1983.

(2) For leading examples of the use of terpenes in chiral synthesis, see: (a) Money, T. *Nat. Prod. Rep.* **1985**, *2*, 253. (b) Money, T. Studies in Natural Products Chemistry. *Stereoselective Synthesis*; Atta-ur-Rahman, Ed.; Elsevier: Amsterdam, 1989; Vol. IV, Part C, p 625. (c) Thomas, A. F.; Bessiere, Y. *Nat. Prod. Rep.* **1989**, *6*, 291. (d) Corey, E. J.; Cheng, X-M. *The Logic of Chemical Synthesis*; John Wiley & Sons: New York, 1989.

0002-7863/91/1513-5765$02.50/0